ChemCatChem

The European Society Journal for Catalysis

Chemistry Europe

European Chemical Societies Publishing

Supported by GECATS GERMAN CATALYSIS SOCIETY

Accepted Article

Title: "Ship-in-a-Bottle" Strategy for Immobilization of 9-Amino(9-deoxy)epi-Cinchona Alkaloid into Molecularly Imprinted Solid Acid: Acetal Hydrolysis/Asymmetric Aldol Tandem Reaction

Authors: Shuai Wei, Jianing Zhang, Shan Li, and Xuebing Ma

To be cited as: *ChemCatChem* 10.1002/cctc.202001402

Link to VoR: https://doi.org/10.1002/cctc.202001402

WILEY-VCH

DOI: 10.1002/cctc.200((will be filled in by the editorial staff))

"Ship-in-a-Bottle" Strategy for Immobilization of 9-Amino(9-deoxy)*epi*-Cinchona Alkaloid into Molecularly Imprinted Solid Acid: Acetal Hydrolysis/Asymmetric Aldol Tandem Reaction

Shuai Wei, Jianing Zhang, Shan Li, Xuebing Ma*

Direct immobilization of versatile 9-amino(9-deoxy)*epi*-cinchona alkaloids without molecule modification to achieve heterogeneous organocatalysis is of interest in the low-cost production of optically active compounds. In this paper, an exquisite "ship-in-a-bottle" strategy for direct and simple immobilization of 9-amino-(9-deoxy)*epi*-quinine ($QNNH_2$) into hollo*w* polystyrene nano-bowl with imprinted free space around -SO_3H was developed *via* acid-base reaction and radical polymerization. The heterogeneous organocatalyst with 0.44 mmol g^{-1} of $QNNH_2$ and 0.48 mmol g^{-1} of residual -SO_3H possessed fast mass transfer due to the characteristic architectural features, such as thin shell thickness, free space around catalytic site, and hollow interior. In heterogeneous acetal hydrolysis/asymmetric aldol tandem reaction, good to excellent catalytic performances (90–95 % yields, *anti/syn* = 88/12–96/4, and 97–99 %ee *anti*) for acetals bearing electron-withdrawing substituents (R = *o, m, p*-NO_2, Cl) were achieved. The "ship-in-a-bottle" $QNNH_2$ displayed good stability and reusability with excellent catalytic performances in the reuses.

Introduction

Over the past decades, asymmetric organocatalysis becomes one of the main tools for the enantioselective synthesis of highly valuable intermediates, fine chemicals, and other bioactive molecules.[1] In spite of strenuous efforts devoted to industrial applications, the contribution of homogeneous asymmetric organocatalysis in the overall production of chiral compounds is much lower than originally expected. The major reason is that the tedious separation of expensive chiral organocatalysts from reaction mixture results in the high-cost production of chiral compounds. From the perspective of green chemistry, a great deal of effort has been devoted to the effective immobilization of various chiral organocatalysts into solid supports through various anchoring mechanisms, including covalent bonding, adsorption/ion-pair forma-tion, encapsulation, and entrapment.[2]

One class of versatile chiral orgaocatalysts, 9-amino(9-deoxy)*epi*-cinchona alkaloids,[3] is widely used in various enantioselective reactions, such as aldol,[4] Michael,[5] epoxidation,[6] Friedel-Crafts alkylation,[7] cycloaddition,[8] *α*-amination,[9] *α*-benzoyloxylation,[10] fluorination,[11] and organocatalytic tandem/domino reaction.[12] To achieve the recovery and reuse of these expensive 9-amino(9-deoxy)*epi*-cinchona alkaloids, two main immobilization strategies, covalent linkage [13] and ion-pair interaction,[14] have been employed for anchoring these organocatalysts into various inorganic [15] and polymeric [16] solid supports. Both the immobilization strategies have their own troublesome drawbacks as well as pleasant advantages. Although the covalent immobilization of 9-amino(9-deoxy)*epi*-cinchona alkaloids into solid supports has become the most often employed method, the high-cost and cumbersome modifications to introduce anchoring point attached to corresponding matrix structure are needed through multistep synthesis and usage of expensive reagents. Meanwhile, it is difficult to achieve good control of well-shaped morphology and porous structure suitable for high effectiveness factors (η) of heterogeneous organocatalysts.[17] Moreover, the most important advantage of ion-pair interaction is fast and direct immobilization of 9-amino(9-deoxy)*epi*-cinchona alkaloids without chemical modification *via* simple acid-base reaction. Nevertheless, owing to the competitive interaction of ionic substrates and salts in reaction medium, the anchored 9-amino(9-deoxy)*epi*-cinchona alkaloids *via* ion-pair interaction usually break off from the framework of catalyst support, resulting in sharp losses of organocatalysts during reaction process. In views of above-mentioned facts, it is highly necessary to develop a simple and straightforward protocol for securely anchoring 9-amino(9-deoxy)*epi*-cinchona alkaloids into solid support, eventually achieving the low-cost production of optically active intermediates and fine chemicals with high catalytic performances in various enantioselective organocatalysis.

In this paper, using 9-amino-(9-deoxy)*epi*-quinine ($QNNH_2$) as an example, a convenient and simple "ship-in-a-bottle" strategy for the entrapment of $QNNH_2$ (ship) into a molecularly imprinted free space around -SO_3H site in hollow bowl-like solid acid (bottle) was developed to overcome the disadvantages of ever-reported immobilization strategies. First, a well-shaped bottle, hollow mesoporous organic nano-bowls PS-SO_3H HMOPBs (PS, polystyrene; HMOPBs, hollow mesoporous organic polymeric

[a] *Shuai Wei, Jianing Zhang, Shan Li, Prof. Xuebing Ma*
College of Chemistry and Chemical Engineering
Southwest University
Chongqing, 400715, P. R. China.
E-mail: zcj123@swu.edu.cn
[+] Shuai Wei and Jianing Zhang contributed equally to this work.

Supporting information for this article is available on the WWW under http://dx.doi.org/10.1002/cctc.200xxxxxx.

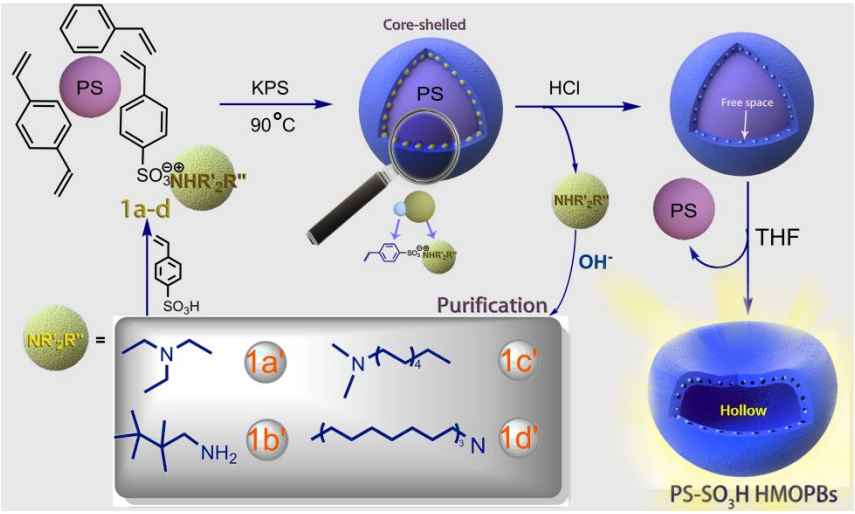

Scheme 1. Schematic illustration for hollow bowl-like solid acid PS-SO_3H HMOPBs with a free space (bottle) around -SO_3H site.

nano-bowls) with free spaces around -SO_3H sites, were fabricated by molecular imprinting method using various amines with different volumes as imprinting molecules. Afterwards, $QNNH_2$ (ship) diffused into the shell of the hollow bowl-like solid acid, and located in the free spaces around -SO_3H sites *via* ion-pair interaction through acid-base reaction between -SO_3H with -NH_2 in $QNNH_2$. Then the as-obtained PS-SO_3H│$QNNH_2$ HMOPBs was dealt with potassium peroxydisulfate solution (KPS) to afford PS-SO_3H‖$QNNH_2$ HMOPBs, in which $QNNH_2$ was further fastened using a carbon chain cable formed by the polymerization of C=C double bonds attached in $QNNH_2$ and polystyrene. The "ship-in-a-bottle" $QNNH_2$, locked firmly in the bottle *via* ion-pair interaction plus covalent linkage, displayed good stability with high catalytic performances in the reuses. In heterogeneous acetal hydrolysis/asymmetric aldol tandem reaction, the heterogeneous organocatalyst exhibited excellent catalytic performances due to the characteristic architectural features, such as mesoporous and thin shell, hollow interior, and well-shaped bowl-like morphology.

Results and Discussion

Fabrication of Solid Acid (bottle) with a Free Space around –SO_3H Site

As shown in Scheme 1, hollow bowl-like solid acid (bottle) with a free space around -SO_3H site, denoted as PS-SO_3H HMOPBs, were prepared through a simple two-step procedure. First, the divinylbenzene (DVB)-cross-linked copolymer of styrene and monomers 1a–d *via* emulsion polymerization was uniformly coated on the surfaces of PS core to prepare solid core-shelled nanospheres. Afterwards, the imprinting molecules 1a'–d' and PS core were eluted with aqueous HCl solution and mixed THF/ethanol sequentially to afford hollow bowl-like PS-SO_3H HMOPBs with a free space around –SO_3H site. It was worth noting that the imprinting molecules 1a'–d' could be recovered and reused. Therefore, the preparation procedure of PS-SO_3H HMOPBs (bottle) was considered to be more simple and convenient than that of ever-reported Poly(St/SO_3H) HMOBs.[16e]

Morphological Control

The effectiveness factor (η) of a catalyst is closely related to morphological features, such as size, shape, and hollow interior.[17] To achieve a high η value, the influences of cross-linker, monomer, imprinting molecule and eluent on the morphological and structural features of solid acids PS-SO_3H HMOPBs were investigated in details. Under the initial conditions: styrene (St, 0.5 mmol) and 1a (1.5 mmol) as polymeric monomers, ethylene glycol dimethyl acrylate (EGDMA, 0.4 mol) as cross-linker, ethanol/THF (*v/v*) = 1/1 as eluents to remove PS core, it was observed that some small beads were attached to the surface of spherical PS-SO_3H HMOPBs due to the out-of-control polymerization without PS template (Figure 1a). Using DVB as a cross-linker instead of EGDMA, the attached beads disappeared (Figure 1b), indicating that DVB could effectively regulate the uniform polymerization of monomers on the surface of PS core. With the decrease in the usage of DVB from 0.4 to 0.2 mol, PS-SO_3H HMOPBs deformed from spherical nanosphere into nano-bowl, which was resulted from the weakened support force of the shell (Figure1c). Upon increasing the usage of DVB from 0.4 to 0.6 mol, some attached beads reappeared (Figure 1d). Furthermore, the volumes of imprinting molecules 1a'–d' played an important role in the morphology of PS-SO_3H HMOPBs. The large 1b'-imprinted PS-SO_3H HMOPBs maintained the similar spherical morphology as small 1a'-imprinted PS-SO_3H HMOPBs (Figure 1f). As the volumes of monomers further increased, 1c'-imprinted PS-SO_3H HMOPBs had a concave shell, and the semi-shells clung closely each other, resulting in no void between two semi-shells (Figure 1g). Unfortunately, the bulky 1d'-imprinted PS-SO_3H HMOPBs cracked into irregular aggregates due to the insufficient supporting force of the perforated shell. In views of good solubility of PS cores in THF, a higher volume ratio of THF to EtOH was better for re-moving PS core to achieve a thinner shell suitable for a high effectiveness factor (η). When the volume ratio of THF to EtOH (*v/v*) increased from 1/1 to 8/1, the more complete removal of PS core produced a thinner shell, and the spherical morphology of 1a'-imprinted PS-SO_3H HMOPBs changed to nano-bowl with no void between two semi-shells due to the weakened supporting force of the thinner shell (Figure 1e). The similar change in shape from hollow nanosphere to nano-bowl was observed for 1b'-imprinted PS-SO_3H HMOPBs. The difference between the two is that 1b'-imprinted bow-like PS-SO_3H HMOPBs showed a deformation with smaller degree, and possessed a void between two semi-shells (Figure 1h). The PS-templated hollow interior in the 1b'-imprinted spherical and bowl-like PS-

SO_3H HMOPBs were clearly evidenced by the TEM images (Figure 2). Based on the mean particle diameters of PS core (327 ± 15 nm, n = 60) and corresponding core-shelled nanosphere (362 ± 28 nm, n = 50), the mean shell thickness of 1b'-imprinted PS-SO_3H HMOPBs was calculated to be about 18 nm. In conclusion, the 1b'-imprinted bowl-like well-shaped PS-SO_3H HMOPBs with hollow interior, thin shell, uniform particle size, and good monodispersity was a desired solid acid or catalyst carrier (bottle) for achieving high effectiveness factor (η). In the following study, 1b'-imprinted PS-SO_3H HMOPBs was selected as model solid acid to investigate its behaviors in adsorption and catalysis.

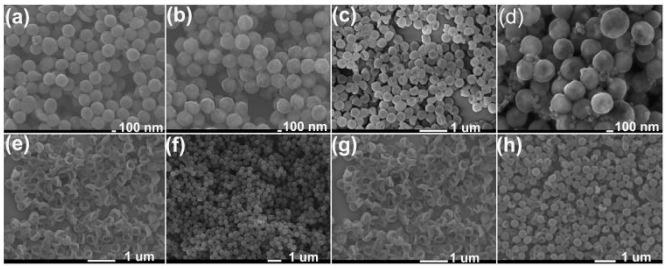

Figure 1. SEM images of solid acids PS-SO_3H HMOPBs using (a) EGDMA, (b) DVB (0.4 mol), (c) DVB (0.2 mol), (d) DVB (0.6 mol) as cross-linkers, (e) ethanol/THF (v/v = 1/8) as eluents to remove PS, (f) 1b' and (g) 1c' as imprinting molecules, (h) ethanol/THF (v/v = 1/8) using 1b' as monomer.

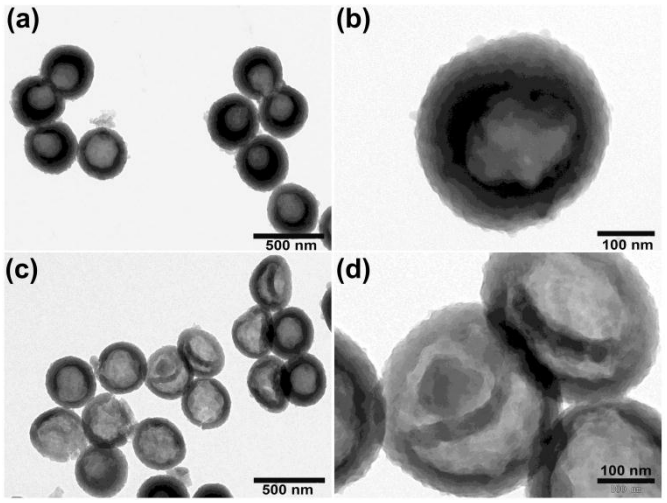

Figure 2. TEM images of 1b'-imprinted PS-SO_3H HMOPBs eluted by mixed THF/EtOH solvents to remove PS core: (a, b) v/v = 1/1 and (c, d) v/v = 8/1.

Imprinted Free Space (bottle) around –SO_3H Site.

As shown in Scheme 1, various organic amines 1a'–d' were used as imprinting molecules to construct free spaces around -SO_3H sites through molecular imprinting strategy, because the amines 1a'–d' could be eluted by aqueous HCl solution from the monomers 1a–d located in the outer shell. From the pore diameter distributions of 1a'–d'-imprinted PS-SO_3H HMOPBs (Figure 3), the different pore diameters of free spaces around -SO_3H sites in the range of 4–30 nm could be constructed. Not as expected, the pore diameter sizes of imprinted free spaces were not proportional to the volumes of imprinting molecules 1a'–d'. The largest amine 1d'-imprinted PS-SO_3H HMOPBs exhibited the lowest desorption D(r) below 5.0 cc g^{-1} with no characteristic mesopores (Figure 3d). As the volumes of imprinting molecules became smaller, the average pore diameters of 1c', 1b', and 1a'-imprinted PS-SO_3H HMOPBs increased from 3.2 to 4.0, 12.7, and 14.9 nm, respectively. The main reason was that the hollowed-out shell, imprinted by larger amine, could not provide enough supporting force and resulted in the collapse of the shell, which was evidenced by the different deformation degrees observed from SEM images (Figure 1b, f, g). Furthermore, it was found that the specific surface areas and pore volumes increased first, and then decreased with the decrease in the volumes of imprinting molecules. Among them, 1b'-imprinted PS-SO_3H HMOPBs possessed the highest specific surface area (97.9 m^2 g^{-1}) and pore volume (0.45 cc g^{-1}), and 1d'-imprinted PS-SO_3H HMOPBs showed the lowest specific surface area (28.3 m^2 g^{-1}) and pore volume (0.13 cc g^{-1}) (Table S1). Unfortunately, a higher specific surface areas, average pore diameter and pore volume of 1b'-imprinted PS-SO_3H HMOPBs were not achieved by varying the molar ratio of 1b/St from 1/1 to 3/1 and 1/3 (Figure S4). Moreover, based on the contents of sulfur in -SO_3H group determined by elemental analysis, 1b'-imprinted PS-SO_3H HMOPBs possessed the higher acid capacity (0.92 mmol g^{-1}) than the others (Table S4). Therefore, it was concluded that the 1b'-imprinted hollow bowl-like PS-SO_3H HMOPBs with the highest specific surface area, pore volume and acid capacity was considered to be the most suitable solid acid with highly effective -SO_3H active sites exposed for adsorption and acid catalysis. Compared with the previously reported Poly(St/SO_3H) HMOBs,[16e] the amine 1b'-imprinted PS-SO_3H HMOPBs provided a perfect porous structure with higher specific surface area and larger pore volume suitable for improving the reactivity of -SO_3H.

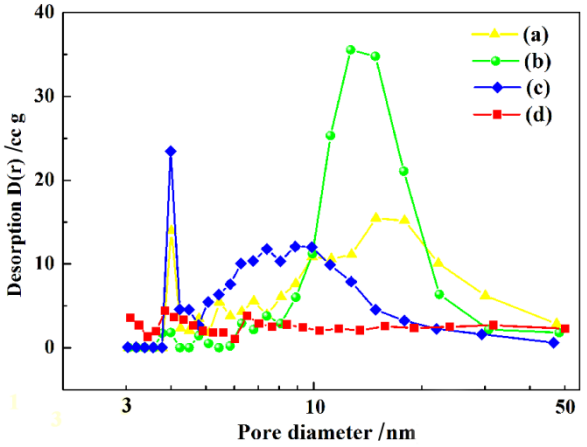

Figure 3. Pore diameter distributions of PS-SO_3H HMOPBs imprinted by different amines: (a) 1a', (b) 1b', (c) 1c', and 1d'.

Different Microenvironments around –SO_3H Site

To elucidate the important role of imprinted free space around-SO_3H in adsorption and acid catalysis, amine 1b'-imprinted solid organic polymeric nanospheres PS-SO_3H OPNs and PS-templated hollow organic polymeric nanospheres PS-SO_3H HOPNs with different microenvironments around -SO_3H sites, were also prepared as contrast solid acids according to the procedures shown in Scheme S1 and Scheme S2, respectively. From the SEM and TEM images (Figure S2), the 1b'-imprinted PS-SO_3H OPNs without PS-templated hollow interior possessed a spherical and solid morphology, and the PS-templated PS-SO_3H HOPNs without 1b' -imprinted free space around -SO_3H site showed a spherical and hollow morphology. Both the contrast solid acids exhibited very low specific surface areas and pore volumes (Figure S5, Table

S3). The low specific surface area and pore volume of PS-SO_3H OPNs were related to the partial elution of imprinting molecule 1b' evidenced by the residual content of nitrogen (0.61 %) (Table S5). Owing to the lack of 1b'-imprinted free space around –SO_3H site, hollow interior in PS-SO_3H HOPNs did not lead to enhanced specific surface area and pore volume. On the surface, both the PS-templated hollow interior and the 1b'-imprinted free space were not so clearly tied to high specific surface area, pore diameter and pore volume. Intrinsically, the combination of hollow interior and imprinted free space around -SO_3H site was essential for solid acid to achieve high specific surface area and pore volume. Elemental analysis indicated that imprinting molecule 1b', located in the thin outer shell of PS-SO_3H HMOPBs with the thickness of 18 nm, could be completely eluted by aqueous HCl solution to imprint free spaces around-SO_3H sites. However, the incomplete elution of deep-buried imprinting molecule 1b' in solid PS-SO_3H OPNs and the dense shell of hollow PS-SO_3H HOPNs without imprinted free spaces resulted in the low specific surface areas and pore volumes.

"Ship-in-a-bottle" $QNNH_2$

As shown in Scheme 2, the "ship-in-a-bottle" immobilization of $QNNH_2$ (ship) into PS-SO_3H HMOPBs (bottle) *via* ion-pair plus covalent linkage to fabricate PS-SO_3H‖$QNNH_2$ HMOPBs was comprised of two convenient and simple steps. First, $QNNH_2$ diffused into the free space around -SO_3H site in the shell of PS-SO_3H HMOPBs and anchored by acid-base reaction of -SO_3H and amino group in $QNNH_2$ to afford PS-SO_3H|$QNNH_2$ HMOPBs, in which $QNNH_2$ was anchored *via* ion-pair interaction. Afterwards, the anchored $QNNH_2$ was further covalently fastened by a carbon chain cable formed through radical polymerization between C=C double bonds attached to $QNNH_2$ and polystyrene. Then, $QNNH_2$ was anchored into the free spaces around -SO_3H sites in the shell of PS-SO_3H‖$QNNH_2$ HMOPBs *via* ion-pair interaction plus covalent linkage.

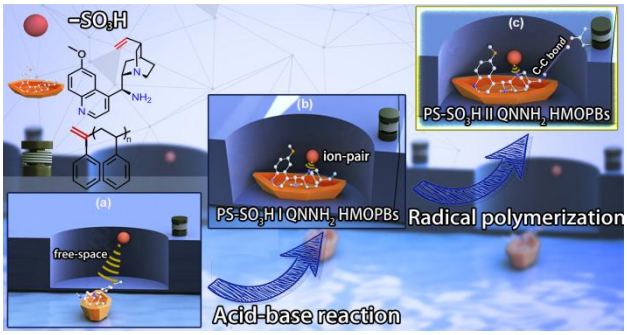

Scheme 2. "Ship-in-a-bottle" immobilization of $QNNH_2$ (ship) into PS-SO_3H HMOPBs (bottle) *via* acid-base reaction and radical polymerization: (a) PS-SO_3H HMOPBs, (b) PS-SO_3H|$QNNH_2$ HMOPBs, and (c) PS-SO_3H‖$QNNH_2$ HMOPBs.

Architectural Feature of PS-SO_3H‖$QNNH_2$ HMOPBs

From the SEM images (Figure 4), all the as-fabricated heterogeneous organocatalysts, including PS-SO_3H‖$QNNH_2$ HMOPBs, PS-SO_3H‖$QNNH_2$ OPNs and PS-SO_3H‖$QNNH_2$ HOPNs, remained their own original bowl-like or spherical morphologies after the immobilization of $QNNH_2$ via acid-base reaction and radical polymerization. Owing to some free spaces around -SO_3H sites occupied by the anchored $QNNH_2$, the specific surface areas and pore volumes slightly decreased to 80.7 m^2 g^{-1} and 0.28 cm^3 g^{-1}, 4.1 m^2 g^{-1} and 0.02 cm^3 g^{-1}, 15.9 m^2 g^{-1} and 0.06 cm^3 g^{-1}, respectively, indicating that there was no significant change in morphology, surface area, and pore volume before and after the immobilization of $QNNH_2$. Based on the architectural features, it was concluded that PS-SO_3H‖$QNNH_2$ HMOPBs could provide the most suitable microenvironment for fast mass transport in heterogeneous organocatalysis.

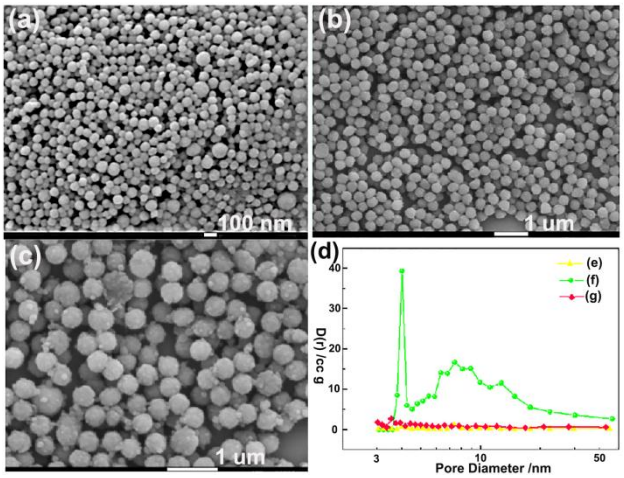

Figure 4. SEM images of (a) PS-SO_3H‖$QNNH_2$ OPNs, (b) PS-SO_3H‖$QNNH_2$ HMOPBs, (c) PS-SO_3H‖$QNNH_2$ HOPNs and (d) pore diameter distributions of (e) PS-SO_3H‖$QNNH_2$ OPNs, (f) PS-SO_3H‖$QNNH_2$ HMOPBs and (g) PS-SO_3H‖$QNNH_2$ HOPNs.

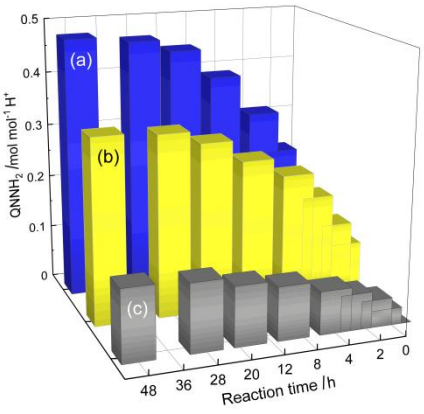

Figure 5. Loading capacities of $QNNH_2$ per mol H^+ versus reaction times: (a) PS-SO_3H|$QNNH_2$ HMOPBs, (b) PS-SO_3H|$QNNH_2$ OPNs, and (c) PS-SO_3H|$QNNH_2$ HOPNs.

Effectiveness of –SO_3H in Immobilization of $QNNH_2$

In order to exclude the effect of polymerization on adsorption, PS-SO_3H|$QNNH_2$ HMOPBs, PS-SO_3H|$QNNH_2$ OPNs, and PS-SO_3H|$QNNH_2$ HOPNs were used to investigate the effectiveness of –SO_3H in the immobilization of $QNNH_2$. According to the sulfur contents determined by elemental analysis, the acid capacities of PS-SO_3H HMOPBs, PS-SO_3H OPNs, and PS-SO_3H HOPNs were calculated to be 0.92, 1.76 and 0.69 mmol g^{-1}, respectively (Table S5). After $QNNH_2$ was anchored *via* ion-pair, the loading $QNNH_2$ in PS-SO_3H|$QNNH_2$ HMOPBs, PS-SO_3H|$QNNH_2$ OPNs, and PS-SO_3H|$QNNH_2$ HOPNs were determined to be 0.44, 0.61, and 0.11 mmol g^{-1} according to the contents of nitrogen, respectively (Table S6). It was found that the adsorption behaviors of $QNNH_2$

into solid acids were closely related to their acid capacities. Among them, PS-SO_3H|$QNNH_2$ OPNs showed a maximal loading capacity of $QNNH_2$ due to the highest acid capacity. In particular, the microenvironment around -SO_3H site was a key influencing factor for the effectiveness of -SO_3H in the immobilization of $QNNH_2$. The term "loading capacity of $QNNH_2$ per mol H^+" was used to describe the effectiveness of -SO_3H. The loading $QNNH_2$ per mol H^+ in various solid acids within 48 h were determined by monitoring the contents of $QNNH_2$ in solution using HPLC. From Figure 5, hollow PS-SO_3H HMOPBs with abundant free spaces around -SO_3H sites exhibited the most effective immobilization of $QNNH_2$, and possessed the highest loading capacity of $QNNH_2$ per mol H^+ (0.48 mol mol^{-1} H^+). Owing to the inferior architectural features to PS-SO_3H HMOPBs, two contrast catalysts, PS-SO_3H|$QNNH_2$ OPNs (0.36 mol mol^{-1} H^+) and PS-SO_3H|$QNNH_2$ HOPNs (0.11 mol mol^{-1} H^+), showed the lower loading capacities of $QNNH_2$ per mol H^+ (Figure 5b, c). Moreover, it was worth noting that the residual -SO_3H had vital functions acting as acid catalysis in the hydrolysis of acetal and synergistic catalyst in asymmetric aldol reaction. Therefore, the molar ratios of anchored $QNNH_2$ to residual -SO_3H in PS-SO_3H|$QNNH_2$ HMOPBs, PS-SO_3H|$QNNH_2$ OPNs, and PS-SO_3H|$QNNH_2$ HOPNs were calculated to be 0.92, 0.56, and 0.12, respectively.

Anchoring Mechanism of "Ship-in-a-bottle" $QNNH_2$

The direct immobilization of $QNNH_2$ into acid-deficient polystyrene through KPS-initiated emulsion polymerization would result in self-polymerization of $QNNH_2$, because it was difficult for $QNNH_2$ to soak into and stay in the pores of the nano-bowl. It was found that the first immobilization of $QNNH_2$ into the free spaces around -SO_3H sites through acid-base reaction to form amine salt was a key step for the immobilization of $QNNH_2$. The successful immobilization of $QNNH_2$ through acid-base reaction between $QNNH_2$ and -SO_3H was confirmed by the IR spectra of PS-SO_3H|$QNNH_2$ HMOPBs with the enhanced =C−H stretching vibrations at 3084, 3057 and 3029 cm^{-1}, out-of-plane bending absorption of terminal =C-H at 964 cm^{-1}, C−H bending vibrations at 1360, 1340 cm^{-1}, and newly emerged characteristic absorption of naphthyl ring at 1603, 1555 cm^{-1}. Furthermore, the formation of amine salt between $QNNH_2$ and -SO_3H was confirmed by the enhanced stretching vibration of S=O at 1122, 1029 cm^{-1} (Figure 5b). To strengthen the stability of $QNNH_2$ in PS-SO_3H|$QNNH_2$ HMOPBs to overcome the loss of $QNNH_2$ *via* weak ion-pair, a carbon chain cable connecting $QNNH_2$ and PS-SO_3H HMOPBs was constructed by dealing PS-SO_3H|$QNNH_2$ HMOPBs with aqueous KPS solution. The formation of the carbon chain cable between $QNNH_2$ and PS-SO_3H HMOPBs through the polymerization of terminal C=C bonds attached in $QNNH_2$ and polystyrene [18] was evidenced by the sharply weakened characteristic absorption of C=C bond and disappeared out-of-plane bending absorption of terminal =C-H, respectively at 1730, 1697, and 964 cm^{-1} (Figure 6c). Therefore, it was confirmed that organocatalyst $QNNH_2$ in PS-SO_3H‖$QNNH_2$ HMOPBs could be anchored via first ion-pair interaction and then covalent linkage.

Stability of "Ship-in-a-bottle" $QNNH_2$

The elution of "ship-in-a-bottle" $QNNH_2$ anchored *via* ion-pair interaction and covalent linkage was investigated by treating PS-SO_3H|$QNNH_2$ HMOPBs and PS-SO_3H‖$QNNH_2$ HMOPBs with 10 mL of aqueous ethanol solution containing HCl (0.01 mol L^{-1}). The amounts of $QNNH_2$ in solution were determined using HPLC. The residual $QNNH_2$ versus elution times were shown in Figure 7.

The residual $QNNH_2$ in PS-SO_3H‖$QNNH_2$ HMOPBs at 48 h was 0.21 mmol g^{-1}. Unfortunately, owing to weak ion-pair interaction between $QNNH_2$ and -SO_3H, the anchored $QNNH_2$ in PS-SO_3H|$QNNH_2$ HMOPBs was completely eluted within 8 h. It is worth noting that the anchored $QNNH_2$ in PS-SO_3H‖$QNNH_2$ HMOPBs was no longer eluted during the time from 8 h to 48 h. This residual $QNNH_2$, about 47.8% of total anchored $QNNH_2$, was considered to be covalently linked to polystyrene by the carbon chain cable. Moreover, some of non-covalently anchored $QNNH_2$ in PS-SO_3H‖$QNNH_2$ HMOPBs displayed a slower rate than those in PS-SO_3H|$QNNH_2$ HMOPBs during 8 h, which was possibly related to two reasons: one was the narrowed mouths of the mesopores in PS-SO_3H HMOPBs (bottle) resulted from the polymerization of terminal C=C bonds attached in polystyrene, and the other was the difficult escape of self-polymerized bulky dimer/trimer of $QNNH_2$ (ship) out from the narrowed mouth of the bottle.

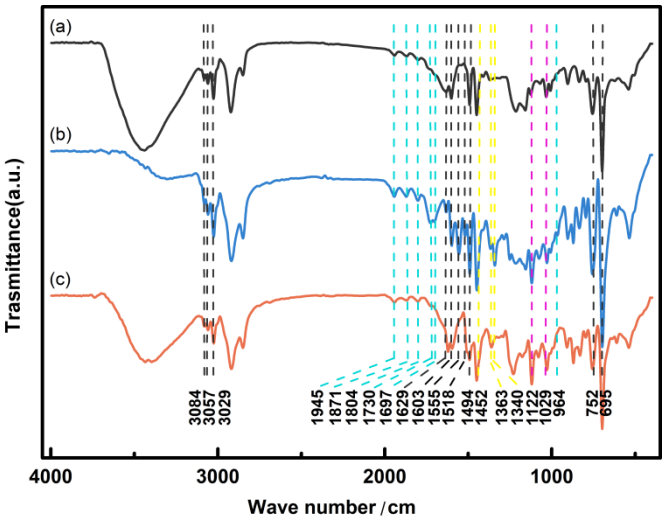

Figure 6. IR spectra of (a) PS-SO_3H HMOPBs, (b) PS-SO_3H|$QNNH_2$ HMOPBs, and (c) PS-SO_3H‖$QNNH_2$ HMOPBs.

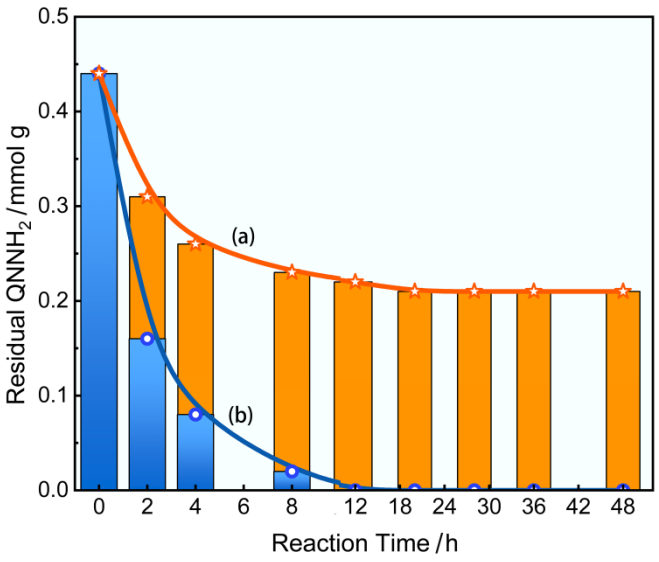

Figure 7. Residual $QNNH_2$ versus elution times: (a) PS-SO_3H‖$QNNH_2$ HMOPBs and (b) PS-SO_3H|$QNNH_2$ HMOPBs.

Catalytic Performances in Acetal Hydrolysis/Asymmetric Aldol Tandem Reaction

Optically active *β*-hydroxyl ketones are one of important intermediates to construct highly valued drug molecules.[19] A new cost-effective synthetic route to optically active *β*-hydroxyl ketones can be achieved through a combination of reactions including acetals from easily available styrene derivatives,[20] hydrolysis of acetals to aromatic aldehydes,[21] and then enantioselective aldol reaction with ketone.[22] With this cost-effective route in mind, a bowl-like multifunctional catalyst was developed to promote heterogeneous one-pot acetal hydrolysis/asymmetric aldol tandem reaction to construct optically pure *β*-hydroxyl ketone.[16e] Herein, a well-shaped hollow bowl-like PS-SO_3H‖$QNNH_2$ HMOPBs with higher specific surface area, pore volume, and more stability of $QNNH_2$ was fabricated to promote heterogeneous one-pot acetal hydrolysis/ asymmetric aldol tandem reaction in a faster reaction rate and a better stereoselectivity.

Table 1. Catalytic performances of various catalysts in acetal hydrolysis/asymmetric aldol tandem reaction [a]

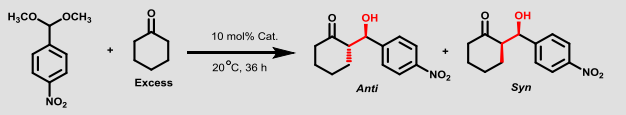

Cat.	Yield (%)[b]	*anti/syn* [c]	%ee [d]
PS-SO_3H ‖ $QNNH_2$ HMOPBs	95	90:10	97
PS-SO_3H ‖ $QNNH_2$ OPNs	67	83:17	91
PS-SO_3H ‖ $QNNH_2$ HOPNs	55	80:20	89
Poly(St/SO_3H-CDNH_2) HMOBs[e]	84	85/15	95

[a] Reaction conditions: Cat. (10.0 mol% of $QNNH_2$), cyclohexanone (1.0 g, 10.0 mmol), 4-$O_2NC_6H_4CH(OCH_3)_2$ (84.0 mg, 0.5 mmol), 20 °C, 1 mL water, 36 h. [b] Isolated yield. [c] Determined by ^{1}H NMR. [d] Determined by HPLC using Daicel Chiralpak AD-H column. [e] 10.0 mol% of $CDNH_2$.[16e]

Table 2. Catalytic performances of various catalysts in acetal hydrolysis/asymmetric aldol tandem reaction[a]

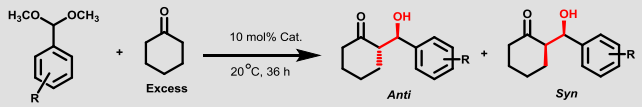

R	Yield (%)[b]	*anti/syn* [c]	%ee [d]
2-NO_2	95	94/6	98
3-NO_2	90	88/12	99
4-NO_2	95	90/10	97
2-Cl	92	90/10	99
3-Cl	91	96/4	98
4-Cl	90	94/6	97
2-CH_3	64	90/10	90
3-CH_3	61	90/10	94
4-CH_3	72	95/5	92
2-OCH_3	42	87/13	94
3-OCH_3	48	82/18	95
4-OCH_3	37	85/15	87

[a] Reaction conditions: PS-SO_3H‖$QNNH_2$ HMOPBs (185.0 mg, 10.0 mol% of $QNNH_2$,11.0 mol% of –SO_3H), cyclohexanone (1.0 g, 10.0 mmol), acetal (0.5 mmol), 20 °C, 1 mL water, 36 h. [b] Isolated yield. [c] Determined by ^{1}H NMR. [d] Determined by HPLC using Daicel Chiralpak AD-H column.

In the tandem reaction of 4-NO_2-$C_6H_4CH(OCH_3)_2$ with cyclohexanone comprising of -SO_3H-catalyzed acetal hydrolysis/-SO_3H and $QNNH_2$-promoted asymmetric aldol addition, the catalytic performances including yields, enantioselectivities, and diastereoselectivities under optimized conditions were listed in Table 1. Compared with ever-reported Poly(St/SO_3H-CDNH_2) HMOBs,[16e] PS-SO_3H‖$QNNH_2$ HMOPBs with higher specific surface area and larger pore volume promo-ted the tandem reaction in higher yield (95%) with better diastereoselectivity (*anti/syn* = 90/10) and enantioselectivity (97% *anti*), due to faster mass transfer. Meanwhile, the reaction time was shortened from 60 to 36 h to achieve the similar yields. However, two contrast catalysts, PS-SO_3H‖$QNNH_2$ OPNs and PS-SO_3H‖$QNNH_2$ HOPNs promoted the tandem reaction in poorer yields and lower enantioselectivities due to lower specific surface areas and pore volumes. These catalytic results indicated that the construction of free spaces around catalytic sites was essential for PS-SO_3H‖$QNNH_2$ HMOPBs to achieve a fast catalytic rate. Moreover, the enhanced $QNNH_2$/-SO_3H-promoted asymmetric aldol reaction could effectively avoid -SO_3H-promoted aldol reaction out of stereochemical control, achieving the better stereoselectivity. Especially, it was worth noting that the increased usage of ever-reported Poly(St/SO_3H-CDNH_2) HMOBs would reduce the stereoselectivity of the product due to its high acid capacity.

Encouraged by the excellent catalytic performances of PS-SO_3H‖$QNNH_2$ HMOPBs in acetal hydrolysis/asymmetric aldol tandem reaction, the scope of acetals was extended to various benzaldehyde methyl acetals bearing electron-withdrawing (R =NO_2 and Cl) and electron-donating groups (R = CH_3 and OCH_3) at the *o*, *m*, *p*-positions. From the catalytic results shown in Table 2, PS-SO_3H‖$QNNH_2$ HMOPBs displayed good to excellent catalytic performances (90–95% yields, *anti/syn* = 88/12–96/4 and 97–99 %ee *anti*) for the acetals bearing electron-withdrawing substituents (R = -NO_2 and -Cl) at *o*, *m* and *p*-positions. The acetals bearing *o*-, *m*- and *p*−CH_3 and OCH_3 electron-donating groups afforded the corresponding *β*-hydroxyl ketones in low to moderate yields (37–72%) with good to excellent stereoselectivities (*anti/syn* = 82/18–95/5 and 87.0–95.0 %ee *anti*). Compared with the ever-reported results, two points were noteworthy about catalytic performances. First, PS-SO_3H‖$QNNH_2$ HMOPBs displayed higher catalytic rates (36 h) to afford corresponding *β*-hydroxyl ketones in enhanced stereoselectivities, due to the higher specific surface area and larger pore volume. Second, the catalytic reaction rates could be further accelerated by increasing the used amount of PS-SO_3H‖$QNNH_2$ HMOPBs. However, due to the higher residual acid capacity (1.77 mmol g^{-1}), the increased amount of Poly(St/SO_3H-CDNH_2) HMOBs resulted in the decreased stereoselectivities, because faster acid-promoted aldol reaction produced the product with no stereochemical control.

Reusability of PS-SO_3H‖$QNNH_2$ HMOPBs

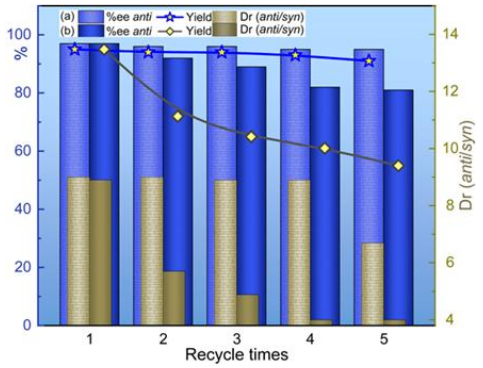

Figure 8. Yields, diastereoselectivities and anantioselectivities of (a) PS-SO_3H‖$QNNH_2$ HMOPBs, and (b) PS-SO_3H|$QNNH_2$ HMOPBs in five recycles.

PS-SO_3H|$QNNH_2$ HMOPBs with high specific surface area (86.5 m^2 g^{-1}) and pore volume (0.34 cm^3 g^{-1}) *via* ion-pair interaction to anchor $QNNH_2$ was used as a contrast catalyst to inves-

tigate the reusability of PS-SO_3H‖$QNNH_2$ HMOPBs with "ship-in-a-bottle" $QNNH_2$ *via* ion-pair interaction plus covalent linkage. Both the catalysts could be recovered by centrifugal separation from reac-tion mixture and directly reused in the next catalytic cycles. The yields, diastereoselectivities and enantioselectivities of PS-SO_3H‖$QNNH_2$ HMOPBs and PS-SO_3H|$QNNH_2$ HMOPBs in the five recycles were listed and shown in Table 3 and Figure 8, respectively. It was found that the 5th-reused PS-SO_3H‖$QNNH_2$ HMOPBs displayed slightly decreased catalytic performances including yield (91%) and stereoselectivity (*anti/syn* = 87/13 and 95 %ee *anti*). Unfortunately, PS-SO_3H|$QNNH_2$ HMOPBs showed a sharply decrease in yield (55%), diastereoselectivity (*anti/syn* =80/20) and enantioselectivity (81 %ee *anti*). To clarify what was driving this difference, SEM, N_2 adsorption-desorption isotherm and elemental analysis were used as tools to characterize the 5th-reused PS-SO_3H|$QNNH_2$ HMOPBs and PS-SO_3H‖$QNNH_2$ HMOPBs. The SEM images showed that both the 5th-reused catalysts maintained their original well-shaped bowl-like morphologies (Figure S6). Owing to the blockage of some mesopores, both the catalysts showed a little decrease in specific surface areas and pore volumes. Then the changes in morphology and porosity were not primary reason for the difference in catalytic performances. Elemental analysis indicated there was a significant difference in nitrogen content. It was found that the nitrogen contents of PS-SO_3H|$QNNH_2$ HMOPBs and PS-SO_3H‖$QNNH_2$ HMOPBs decreased from 0.61 to 0.33% and from 0.59 to 0.54%, respectively. The sharp loss of $QNNH_2$ out from PS-SO_3H|$QNNH_2$ was closely related to the weak ion-pair interaction between $QNNH_2$ and PS-SO_3H HMOPBs. After $QNNH_2$ was further fastened via a carbon chain cable in PS-SO_3H‖$QNNH_2$ HMOPBs, the stability of $QNNH_2$ in the reuses was significantly improved, which was verified by the elution results in aqueous HCl solution (Figure 7). Therefore, the covalent linkage of $QNNH_2$ was responsible for the good stability of PS-SO_3H‖$QNNH_2$ HMOPBs in the reuses.

Table 3. Catalytic performances of reused PS-SO_3H‖$QNNH_2$ HMOPBs and PS-SO_3H|$QNNH_2$ HMOPBs in acetal hydrolysis/asymmetric aldol tandem reaction [a]

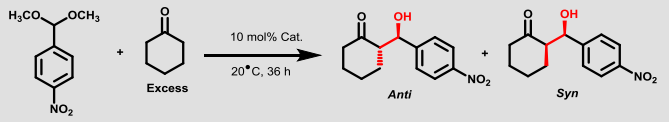

Cycles	Cat.	Yield (%)[b]	*anti/syn* [c]	%ee [d]
1	A[e]	95	97	90:10
	B[f]	95	97	89:11
2	A	94	96	90:10
	B	72	92	85:15
3	A	94	96	89:11
	B	65	89	83:17
4	A	93	95	87:13
	B	61	82	80:20
5	A	91	95	87:13
	B	55	81	80:20

[a] Reaction conditions: cyclohexanone (1.0 g, 10.0 mmol), acetal (98.5 mg, 0.5 mmol), 20 °C, 1 mL water, 36 h. [b] Isolated yield. [c] Determined by ^{1}H NMR. [d] Determined by HPLC using Daicel Chiralpak AD-H column. [e] PS-SO_3H‖$QNNH_2$ HMOPBs. [f] PS-SO_3H|$QNNH_2$ HMOPBs.

Conclusion

Direct and simple immobilization of versatile 9-amino(9-deoxy) *epi*-cinchona alkaloids *via* acid-base reaction without molecule modification as heterogeneous organocatalyst is of economic interest in the low-cost production of numerous optically active compounds. However, the weak ion-pair interaction leads to the easy elution of 9-amino(9-deoxy)*epi*-cinchona alkaloids in catalytic process, which severely limits its industrial applications. In this study, we developed a "ship-in-a-bottle" strategy for direct and simple immobilization of $QNNH_2$ into molecularly imprinted solid acid via ion-pair interaction through acid-base reaction plus covalent linkage through radical polymerization. This "ship-in-a-bottle" immobilization strategy had some inbuilt advantages over ever-reported heterogeneous 9-amino(9-deoxy) *epi*-cinchona alkaloids, such as simple immobilization without molecular modification, controllable architectural feature, and low-cost procedure. The as-fabricated heterogeneous organocatalyst, acting as acid catalysis and cooperative catalysis of -SO_3H/$QNNH_2$, possessed a fast mass transfer in heterogeneous organocatalysis owing to thin shell thickness, free space around catalytic site, and hollow interior. Exemplified in heterogeneous acetal hydrolysis/asymmetric aldol tandem reaction, good to excellent catalytic performances including yield and stereoselectivity were achieved due to its superior characteristic architectural features. In conclusion, this work sheds new light on heterogeneous organocatalyst about how to anchor 9-amino(9-deoxy)*epi*-cinchona alkaloids in a low-cost and convenient way.

Experimental Section

Materials and Characterization

Styrene was purified by distillation under reduced pressure before use. Polystyrene cores (PS, d = 327 ± 15 nm, *n* = 60) were prepared according to the reference,[16c] and their SEM image and particle size distribution were shown in Figure S1. 4-Vinylbenzenesulfonate salt monomers 1a-d were synthesized according to the procedues shown in ESI#. The contrast solid acids, amine-imprinted organic polymeric nanospheres PS-SO_3H OPNs (PS, polystyrene; OPNs, organic polymeric nanospheres, Scheme S1) and PS-templated hollow organic polymeric nanospher-es PS-SO_3H HOPNs (PS, polystyrene; HOPNs, hollow organic polymeric nanospheres, Scheme S2), were prepared according to the procedures shown in ESI#. The other chemicals were used as received without any further purification.

The chemical structures of products in acetal hydrolysis/ asymmetric aldol tandem reaction were confirmed by ^{1}H NMR spectra on a Bruker av-600 NMR instrument, in which all chemical shifts were reported down-field in ppm relative to the hydrogen resonance of TMS. Elemental analysis was carried out on a vario Micro cube elemental analyzer. The morphology of sample was observed by SM-7800F scanning electron microscopy (SEM) and Tecnai G2 F20 transmission electron microscopy (TEM), operated at 10 kV and 200 kV, respectively. N_2 adsorption–desorption isotherms were performed at 77.4 K on Autosorb-1 apparatus, in which sample was degassed at 105 °C for 12 h before measurement. The BET surface areas were calculated from the adsorption data in the relative pressures P/P_0 (0.05−0.30), and the pore diameter distributions and pore volumes were obtained from desorption branches using BJH method. FT-IR spectroscopy was performed on a Perkin-Elmer model GX spectrometer using KBr pellet. The *anti/syn* ratios of products were detected by ^{1} H NMR according to the peak area ratios of proton in −CHOH group, and the enantiomeric excesses (%ee) were monitored by Agilent LC-1200 HPLC with a 254 nm UV-vis detector using chiral Daicel Chiralpak AD-H column (4.6 mm × 25 cm), eluting with *n*-hexane/*iso*-propanol under 20°C.

Preparation of Molecularly Imprinted Solid Acid PS-SO_3H HMOPBs

In Ar-filled round-bottom flask (100 mL), PS cores (200 mg, *d* = 327 ± 11 nm, *n* = 60) were ultrasonically dispersed in ethanol (2 mL) for 5 min, added deionized water containing 0.5%wt PVA (10 mL), and

stirred at room temperature for 24 h to afford a suspension of PS cores. In another Ar-filled three-necked flask (100 mL), a mixture of aqueous 2, 2, 3, 3-tetramethylbutan-1-aminium 4-vinylbenzenesulfonate 1b (471.4 mg, 1.5 mmol, 3 mL) solution, ethanol styrene solution (52.0 mg, 0.5 mmol, 1 mL), and deionized water containing 0.5% wt PVA (10 mL) was ultrasonically dispersed for 30 min, and the suspension of PS cores was injected by syringe. After being stirred for 4 h, KPS (27.0 mg, 0.1 mmol, 4 mL) and DVB (52.1 mg, 0.4 mmol, 1 mL) were added quickly. The reaction mixture was heated to 90 °C, stirred for 18 h, cooled to room temperature, and separated by centrifugation. The isolated solid was washed successively with deionized water (8 mL × 3) and ethanol (10 mL × 3), and then stirred in aqueous HCl solution (3 mol L^{-1}, 8 mL) at room temperature for 12 h to remove the imprinting molecule 1b'. The isolated solid was treated twice with hydrochloric acid to completely remove 1b'. The eluted hydrochloride of 1b' was recovered by neutralization with NaOH solution and extraction with toluene. The 1b'-imprinted solid acid was dispersed in mixed THF/ethanol solvents (*v/v* = 8/1, 8 mL) at room tempe-rature for 12 h to remove PS cores. The procedure was repeated several times until the turbid phenomenon was not observed upon adding the THF/ethanol solution into water, indicating the complete removal of PS cores. The as-obtained white powder was dried naturally to afford PS-SO_3H HMOPBs with imprinted free spaces around -SO_3H sites (288 mg, 76%).

"Ship-in-a-bottle" Preparation of PS-SO_3H‖$QNNH_2$ HMOPBs

After solid acid PS-SO_3H HMOPBs (370 mg) was well-dispersed in dioxane (10 mL) for 30 min, $QNNH_2$ (64.7 mg, 0.2 mmol) was added and stirred at room temperature for 12 h. The isolated faint yellow solid PS-SO_3H⏐$QNNH_2$ HMOPBs was re-dispersed in ethanol (2 mL) under ultrasonic radiation, added deionized water containing 0.5%wt PVA (10 mL), and stirred at room temperature for 24 h. To the suspension of PS-SO_3H⏐$QNNH_2$ HMOPBs was added aqueous KPS solution (27 mg, 0.1 mmol, 4 mL), heated to 90 °C, and stirred for 36 h. The isolated solid was washed with dioxane (10 mL × 3) and dried naturally to afford PS-SO_3H‖$QNNH_2$ HMOPBs (357.5 mg) with "ship-in-a-bottle" $QNNH_2$.

According to the same procedure as PS-SO_3H‖$QNNH_2$ HMOPBs, two contrast catalysts, PS-SO_3H‖$QNNH_2$ OPNs and PS-SO_3H‖$QNNH_2$ HOPNs with anchored $QNNH_2$ *via* ion-pair plus covalent linkage, were also prepared by using solid acids PS-SO_3H OPNs and PS-SO_3H HOPNs, respectively.

Heterogeneous Acetal Hydrolysis/asymmetric Aldol Tandem Reaction

The mixture of PS-SO_3H‖$QNNH_2$ HMOPBs (185.0 mg, 10.0 mol% of $QNNH_2$ and11.0 mol% of -SO_3H), cyclohexanone (1.0 g, 10.0 mmol), and deionized water (1.0 mL) was stirred at 20 °C for 15 min, and added 4-nitrobenzaldehyde dimethyl acetal (168.1 mg, 1.0 mmol). After the resulting mixture was stirred at 20 °C for 24 h, the catalyst was separated by centrifugation. The recovered catalyst was reused directly for the next catalytic cycle. The centrifugate was extracted by ethyl acetate (20 mL × 3). The combined organic phases were dried over anhydrous Na_2SO_4, filtered and evaporated to afford crude product. The crude product was purified by silica gel column chromatography using petroleum ether/ethyl acetate (*v/v* = 10/1 → 2/1) as eluents to afford the pure aldol adduct (118.6 mg, 95%) with *anti/syn* = 90/10 and 97.0 %ee *anti*.

Acknowledgements

This work was supported by National Natural Science Foundation of China [51973177], and Basic Science and Advanced Technology Research Project of Chongqing Science&Technology commission, P. R. China (cstc 2017jcyjBX0027).

Keywords: 9-Amino(9-deoxy)*epi*-cinchona alkaloid • Heterogeneous organocatalysis • Hollow nanosphere • Solid acid • Acetal hydrolysis/asymmetric aldol tandem reaction

[1] a) A. Przydacz, A. Skrzyńska, Ł. Albrecht, *Angew. Chem. Int. Ed.* **2019**, *58*, 63–73; b) P. W. Xu, J. S. Yu, C. Chen, Z. Y. Cao, F. Zhou, J. Zhou, *ACS Catal*. **2019**, *9*, 1820−1882; c) X. Xie, L. Xiang, C. Peng, B. Han, *Chem. Rec*., **2019**, *19*, 2209−2235; d) S. Meninno, C. Volpe, A. Lattanzi, *ChemCatChem* **2019**, *11*, 3714−3727.

[2] a) M. Ferré, R. Pleixats, M. W. C. Man, X. Cattoën, *Green Chem*. **2016**, *18*, 881−922; b) S. Itsuno, M. M. Hassan, *RSC Adv*. 2014, *4*, 52023−52043; c) L. Zhang, S. Z. Luo, J. P. Cheng, *Catal. Sci. Technol*. **2011**, *1*, 507−516; d) B. Ni, A. D. Headley, *Chem. Eur. J*. **2010**, *16*, 4426−4436.

[3] a) J. D. Duan, P. F. Li, *Catal. Sci. Technol*. **2014**, *4*, 311−320; b) P. Melchiorre, *Angew. Chem. Int. Ed*. **2012**, *51*, 9748−9770; c) L. Jiang, Y. C. Chen, *Catal. Sci. Technol.* **2011**, *1*, 354−365; d) L. W. Xu, J. Luo, Y. X. Lu, *Chem. Commun*. **2009**, 1807−1821; e) T. Marcelli, H. Hiemstra, *Synthesis* **2010**, *8*, 1229−1279.

[4] a) Y. H. Lam, K. N. Houk, *J. Am. Chem. Soc*. **2015**, *137*, 2116−2127; b) C. Liu, Q. Zhu, K. W. Huang, Y. X. Lu, *Org. Lett*. **2011**, *13*, 2638−2641.

[5] a) J. W. Xie, W. Chen, R. Li, R. M. Zeng, W. Du, L. Yue, Y. C. Chen, Y. Wu, J. Zhu, J. G. Deng, *Angew. Chem. Int. Ed*. **2007**, *46*, 389−392; b) P. F. Li, Y.C. Wang, X. M. Liang, J. X. Ye, *Chem. Commun*. **2008**, 3302−3304; c) Z. G. Yang, J. Liu, X. H. Liu, Z. Wang, X. M. Feng, Z. S. Su, C. W . Hu, *Adv. Synth. Catal*. **2008**, *350*, 2001−2006; d) Q. Zhu, L. L. Cheng, Y. X. Lu, *Chem. Commun*. **2008**, 6315−6317.

[6] a) O. Lifchits, M. Mahlau, C. M. Reisinger, A. Lee, C. Farès, I. Polyak, G. Gopakumar, W. Thiel, B. List, *J. Am. Chem. Soc*. **2013**, *135*, 6677−6693; b) X. J. Lu, Y. Liu, B. F. Sun, B. Cindric, L. Deng, *J. Am. Chem. Soc*. **2008**, *130*, 8134−8135; c) C. M. Reisinger, X. W. Wang, B. List, *Angew. Chem. Int. Ed*. **2008**, *47*, 8112−8115.

[7] A. A. Hamilton, C. Bo, P. Melchiorre, *J. Am. Chem. Soc*. **2013**, *135*, 9091−909.

[8] a) Q. Q. Yang, X. Yin, X. L. He, W. Du, Y. C. Chen, *ACS Catal*. **2019**, *9*, 1258−1263; b) P. Yu, C. Q. He, A. Simon, W. Li, R. Mose, M. K. Thøgersen, K. A. Jørgensen, K. N. Houk, *J. Am. Chem. Soc*. 2018, **140**, 13726−13735.

[9] C. Liu, Q. Zhu, K. W. Huang, Y. X. Lu, *Org. Lett*. **2011**, *15*, 2638−2641.

[10] O. Lifchits, N. Demoulin, B. List, *Angew. Chem. Int. Ed*. **2011**, *50*, 9680−9683.

[11] a) Y. H. Lam, K. N. Houk, *J. Am. Chem. Soc*. **2014**, *136*, 9556−9559; b) P. Kwiatkowski, T. D. Beeson, J. C. Conrad, D. W. C. MacMillan, *J. Am. Chem. Soc*. **2011**, *133*, 1738−1741.

[12] a) T. Chanda, J. C. G. Zhao, *Adv. Synth. Catal*. **2018**, *360*, 2-79; b) H. Z. Yang, Q. Q. Wang, Y. Luo, L. Ye, X. Y. Li, F. Chen, Z. G. Zhao, X. F. Li, *Org. Biomol. Chem*. **2020**, *18*, 1607−1611; c) B. Mondal, M. Balha, S. C. Pan, *Org. Biomol. Chem*. **2019**, *17*, 7849−7853; d) H. J. Lee, C. W. Cho, *J. Org. Chem*. **2013**, *78*, 3306−3312; e) X. Feng, Z. Zhou, R. Zhou, Q. Q. Zhou, L. Dong, Y. C. Chen, *J. Am. Chem. Soc*. **2012**, *134*, 19942−19947; f) P. Galzerano, F. Pesciaioli, A. Mazzanti, G. Bartoli, P. Melchiorre, *Angew. Chem. Int. Ed*. **2009**, *48*, 7892−7894.

[13] A. F. Trindade, P. M. P. Gois, C. A. M. Afonso, *Chem. Rev*. **2009**, *109*, 418−514.

[14] a) P. Barbaro, F. Liguori, *Chem. Rev*. **2009**, *109*, 515−529; b) J. M. Fraile, J. I. García, J. A. Mayoral, *Chem. Rev*. **2009**, *109*, 360−417.

[15] a) R. Porta, M. Benaglia, F. Coccia, F. Cozzi, A. Puglisi, *Adv. Synth. Catal*. **2015**, *357*, 377−383; b) L. W. Zhao, Y. P. Li, P. Yu, X. Han, J. He, *ACS Catal*. **2012**, *2*, 1118−1126; c) J. W. Wan, L. ding, T. Wu, X. B. Ma, Q. Tang, *RSC Adv*. **2014**, *4*, 38323−38333; d) A. Ciogli, D. Capitani, N. D. Iorio, S. Crotti, G. Bencivenni, M. P. Donzello, C. Villani, *Eur. J. Org. Chem*. **2019**, 2020−2028; e) D. A. Aguiler, L. S. Di Sante, A. Pettignano, R. Riccioli, J. Roeske, L. Albergati, *Eur. J. Org. Chem*. **2019**, 3842−3849; f) M. Nazish, G. Kumar, R. Tak, N. U. H. Khan, R. I. Kureshy, *ChemistrySelect* **2018**, *3*, 7394−7401; g) T. Wu, D. D. Feng, G. X. Xie, X. B. Ma, *RSC Adv*. **2016**, *6*, 77396−77405.

[16] a) G. X. Xie, J. N. Zhang, X. B. Ma, *ACS Catal*. **2019**, *9*, 9081−9086; b) G. X. Xie, J. K. Tian, S. Wei, X. Z. Liu, X. B. Ma, *Appl. Catal., A* **2018**, *565*, 87−97; c) J. Izquierdo, C. Ayats, A. H. Henseler, M. A. Pericàs, *Org. Biomol. Chem.* **2015**, *13*, 4204−4209; d) G. X. Xie, S. Wei, L. Zhang, X. B. Ma, *Ind. Eng. Chem. Res*. **2019**, *58*, 2812−2823; e) Y. N. Bo, X. R.

Wang, X. T. Deng, X. B. Ma, *Appl. Catal., A* **2020**, *590*, 117360; f) R. Porta, F. Coccia, R. Annunziata, A. Puglis, *ChemCatChem* **2015**, *7*, 1490−1499; g) S. H. Youk, S. H. Oh, H. S. Rho, J. E. Lee, J. W. Lee, C. E. Song, *Chem. Commun*. **2009**, 2220−2222; h) H. Y. Zhang, W. T. Yang, J. P. Deng, *Polymer* **2015**, *80*, 115−122.

[17] a) S. W. Cao, F. Tao, Y. Tang, Y. T. Li, J. G. Yu, *Chem. Soc. Rev*. **2016**, *45*, 4747−4765; b) L. Zhang, J. N. Zhang, S. Wei, S. Li, X. B. Ma, *Appl. Catal., A* **2020**, *600*, 117560; c) Z. W. Zhao, D. D. Feng, G. X. Xie, X. B. Ma, *J. Catal*. **2018**, *359*, 36−45; d) F. Q. Dai, Z. W. Zhao, G. X. Xie, D. D. Feng, X. B. Ma, *ChemCatChem* **2017**, *9*, 89−93.

[18] a) F. Lin, Z. H. Liu, M. Y. Wang, B. Liu, S. H. Li, D. M. Cui, *Angew. Chem. Int. Ed.* **2020**, *59*, 4324−4328; b) Z. H. Liu, C. G. Yao, C. J. Wu, Z. F. Zhao, D. M. Cui, *Macromolecules* **2020**, *53*, 1205−1211.

[19] Y. Yamashita, T. Yasukawa, W. J. Yoo, T. Kitanosono, S. Kobayash, *Chem. Soc. Rev*. **2018**, *47*, 4388−4480.

[20] R. Ray, A. D. Chowdhury, G. K. Lahiri, *ChemCatChem* **2013**, *5*, 2158–2161.

[21] a) L. C. Lee, J. Lu, M. Weck, C. W. Jones, *ACS Catal*. **2016**, *6*, 784−787; b) D. Vernekar, D. Jagadeesan, *Catal. Sci. Technol*. **2015**, *5*, 4029−4038.

[22] a) M. Duss, L. S. Manni, L. Moser, S. Handschin, R. Mezzenga, H. J. Jessen, E. M. Landau, *ACS Appl. Mater. Interfaces* **2018**, *10*, 5114−5124; b) Y. Wang, H. F. Shen, L. Zhou, F. Y. Hu, S. L. Xie, L. M. Jiang, *Catal. Sci. Technol*. **2016**, *6*, 6739−6749; c) X. Feng, H. S. Jena, K. Leus, G. B. Wang, J. Ouwehand, P. Van der Voort, *J. Catal*. **2018**, *365*, 36−42; d) G. X. Xie, D. D. Feng, X. B. Ma, *Mol. Catal*. **2017**, *434*, 86−95; e) L. Lan, G. X. Xie, T. Wu, D. D. Feng, X. B. Ma, *RSC Adv*. **2016**, *6*, 55894−55902; f) J. Q. Zhou, J. W. Wan, X. B. Ma, W. Wan, *Org. Biomol. Chem*. **2012**, *10*, 4179−4185; g) W. Wang, X. B. Ma, J. W. Wan, J. Cao, Q. Tang, *Dalton Trans*. **2012**, *41*, 5715−5726.

Received: ((will be filled in by the editorial staff))
Published online: ((will be filled in by the editorial staff))

10.1002/cctc.202001402

Entry for the Table of Contents

FULL PAPER

"Ship-in-a-bottle" strategy for the direct immobilization of 9-amino(9-deoxy)*epi*-cinchona alkaloid into molecularly imprinted hollow solid acid without molecular modification was developed *via* simple acid-base reaction and radical polymerization. Good to excellent catalytic performances, including yield and stereoselectivity, were achieved in heterogeneous acetal hydrolysis/ asymmetric aldol tandem reaction due to its hollow and mesoporous characteristic architectural features.

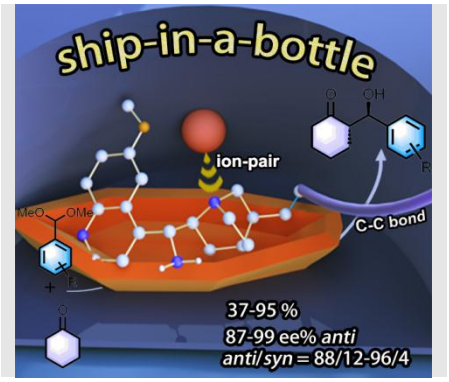

*Shuai Wei, Jianing Zhang, Shan Li, Xuebing Ma**

Page No. – Page No.

"Ship-in-a-Bottle" Strategy for the Immobilization of 9-Amino(9-deoxy)*epi*-Cinchona Alkaloid into Molecularly Imprinted Solid Acid: Exemplified for Acetal Hydrolysis/Asymmetric Aldol Tandem Reaction